

SUPPLEMENTARY EXPERIMENTAL PROCEDURES

Assembly and purification of the DNA duplexes

DNA duplexes were assembled from oligodeoxyribonucleotides (Integrated DNA Technologies; see Table S1 for the sequences) that were purified by denaturing polyacrylamide gel electrophoresis (PAGE) before use.

The DNA oligonucleotide used to create DNA dumbbells was first 5'-phosphorylated using γ -[³²P]ATP (MP Biomedicals) and T4-polynucleotide kinase (NEB) according to the supplier's instructions. The reaction mixture was buffer exchanged over a Biospin 6 column (Bio-Rad) into annealing buffer [5 mM Tris-HCl, pH 8.0, 25 mM NaCl, 0.5 mM Na-EDTA]. The oligodeoxyribonucleotide, which is self-complementary, was annealed by heating the mixture to 90 °C and cooling to room temperature over two hours. T4 DNA ligase (1000 units per 80 pmol oligodeoxyribonucleotide; NEB) together with the supplier's T4 DNA ligase buffer was added, and ligation was carried out for three min at room temperature. The reaction mixture was buffer exchanged over a Biospin 6 column into 8.5 M urea, 20% sucrose, 5 mM Na-EDTA and heated for 45 s at 90 °C. DNA dumbbells were separated from unligated oligodeoxyribonucleotides by denaturing PAGE (14%). Purified DNA dumbbells were eluted from gel slices in 10 mM Tris-HCl pH 8.0, 50 mM NaCl, 1 mM Na-EDTA.

The other DNA duplexes (Table S1) were formed by annealing of complementary oligodeoxyribonucleotides as described above. As necessary, the duplexes were 5'-phosphorylated with [³²P]ATP and T4-polynucleotide kinase and purified by non-denaturing PAGE.

SUPPLEMENTARY RESULTS

DNA dumbbell duplexes are cleaved slightly less efficiently than blunt-end duplexes of the same sequence

Under conditions that allow all DNA molecules to be bound by the enzyme (with saturating enzyme concentrations and enzyme in excess of DNA), the dumbbell DNA duplex was cleaved less efficiently at equilibrium than the corresponding DNA duplex without terminal triethylene glycol linkers. Approximately 15% or 10% more DNA cleavage was observed with duplexes that did not have the terminal linkers in the absence or presence of saturating concentrations of AMPPNP, respectively (data not shown). Two non-mutually exclusive models can account for the observation that the dumbbell DNA duplex is cleaved less efficiently than its blunt-ended counterpart.

The first model posits that the cleavage equilibria are unperturbed by the presence of the terminal linkers but that some of the DNA dumbbells (~10%, analysis not shown) cannot be cleaved or are not available for cleavage. For example, the DNA dumbbells could be covalently or non-covalently heterogeneous, and one population of the DNA dumbbells cannot be cleaved. Because the DNA dumbbells are perfectly palindromic and the termini are covalently linked an alternative secondary structure could be adopted by a fraction of the dumbbell population in which the triethylene glycol linkers are now in the middle as opposed to the ends of the duplex. It is very likely that this alternative secondary structure would not be cleavable by the enzyme. Also, covalent heterogeneity of the DNA dumbbell population cannot be ruled out, although great care was taken during the purification of the 68 nucleotides long DNA oligonucleotide from which the DNA 34 bp dumbbell was constructed (see Table S1 for the sequence). The oligonucleotide was purified twice by PAGE including one strongly denaturing (40% formamide, 7 M urea) gel that eliminated residual secondary structure of the self-complementary sequence. Alternatively, the presence of the terminal linkers may favor unproductive binding of the duplex to the enzyme. For example, the linkers may favor binding of the duplex in a different register or at an alternative binding site relative to a duplex without the linkers. Such unproductive binding of the DNA dumbbell would reduce the observed extent of cleavage because

at any given time only a fraction of DNA dumbbells are bound at the DNA cleavage site in a cleavage competent manner.

In the second model, the DNA cleavage equilibria are lowered by the presence of the terminal linkers. For example, the linkers could make interactions with the enzyme that allosterically influence DNA cleavage, or they could prevent interactions of the DNA with the enzyme that are important for DNA cleavage. A number of observations argue against such a model. First, the DNA affinities of the DNA dumbbell and the corresponding blunt-end duplex are the same, within 50% (measured under conditions of the cleavage assay; data not shown), suggesting that the terminal linkers do not grossly affect interactions formed between the enzyme and the DNA. Second, a dumbbell made with chemically distinct terminal linkers (5 thymidine nucleotides) was also cleaved less efficiently than the corresponding blunt-end DNA duplex (data not shown). This observation indicates that the decreased cleavage of DNA dumbbells is not specific to the chemical identity of the terminal linkers. Lastly, DNA cleavage is only modestly influenced by changes in the DNA sequence at positions outside the central 20 bp of the cleavage site [1]. DNA-protein interactions that are important for cleavage are therefore not expected to be perturbed by the presence of the terminal linkers of the 34 bp DNA dumbbell duplex.

In summary, a number of observations argue against the second model, whereas it is plausible that a fraction of the dumbbells are not cleavable or are unavailable for DNA cleavage -e.g., through formation of an alternative secondary structure (model 1). We have therefore corrected the fraction of DNA dumbbells that are cleavable and available for cleavage in the quantitative analysis of the DNA cleavage reaction by 10%.

Models that do not postulate the existence of two enzyme species do not account for the observed DNA binding and release kinetics

We show in the Results and Discussion that the DNA binding and dissociation kinetics in the presence of AMPPNP is consistent with a model that postulates the existence of two enzyme species. In this section we consider alternative mechanisms

that do not postulate the existence of two enzyme species. In particular, we discuss if multiple DNA binding sites or if heterogeneity of the DNA instead of heterogeneity of the enzyme could account for the data. We examine the consistency of these models with the DNA binding and dissociation data collected in the presence of Mg^{2+} (Figs. 5A & 6A) because the DNA binding and dissociation kinetics are not complicated by DNA cleavage under those conditions. This analysis indicates that there exist at least two enzyme species. Analogous conclusions hold for the dataset collected in Ca^{2+} that contain the additional cleavage steps (Figs. 5B & 6B).

Heterogeneity of the fluorophore-labeled DNA does not account for the observed DNA binding kinetics

The model depicted in Scheme S6A postulates that heterogeneity (covalent or conformational) of the fluorophore-labeled DNA exists (DNA species S_1 and S_2). The following arguments show that this model cannot account for the slowest DNA association phase with a positive amplitude ($k_3 = 0.04$ and 0.13 s^{-1} ; Fig. 5A). If the model were true then the amplitudes of the slowest phase relative to the other phases should stay constant as long as the enzyme concentration is kept in excess of the DNA concentration. Counter to this prediction, the amplitude of the slowest phase decreased when the enzyme-DNA ratio was increased above one, and the slow phase was undetectable when the enzyme concentration exceeded six-times the DNA concentration (Fig. 5). Thus, two or more different DNA species cannot account for the observed DNA binding kinetics.

The presence of two different DNA binding sites does not account for the observed DNA binding and release kinetics

In this section we test the consistency of the model in Scheme S6B with the observed DNA binding and release kinetics. The model postulates that the enzyme has two DNA binding sites that could be occupied under the conditions of our experiments. If these binding sites bound DNA with different rate constants, multiphasic DNA binding and release kinetics could be observed. Two subsets of

models must be considered. Either the two species E^S and E_S have similar fluorescence anisotropy values (Scenario 1) or they do not (Scenario 2). A discussion of these models follows.

Scenario 1: If both enzyme-DNA species have similar fluorescence anisotropy values then two phases in the DNA binding time traces can only be obtained with $[E] \geq [DNA]$ if the following conditions are met: K_{d1} equilibrates faster than K_{d2} and the chosen concentrations are saturating for K_{d2} but not fully saturating for K_{d1} . Under those conditions a fraction of the DNA would bind fast to the site designated by K_{d1} . The slow phase arises through slow but complete DNA binding to the site designated by K_{d2} . In this model, E^S would be formed with the observed rate constant of the slow DNA association phase ($k_3 = 0.04 - 0.13 \text{ s}^{-1}$; Fig. 5A). However, formation of E^S is too slow to account for the observation that a slowly dissociating enzyme-DNA species has already build up to approximately 50% after 65 ms (Fig. 6A), which corresponds to an observed rate constant of $\ln(2) / 0.065 \text{ s} = 11 \text{ s}^{-1}$, thereby providing evidence against this model.

Scenario 2: The second subset of models assumes that the enzyme concentration is saturating for both binding sites but that E_S in Scheme S6B has a significantly lower fluorescence anisotropy than E^S . A slow phase in the DNA binding time traces can arise if E^S (the low anisotropy complex) initially builds up before also E_S (the high anisotropy complex) is formed. For enzyme concentrations that are equal to the DNA concentrations, the ratio of the amplitudes between the fast and the slow phases are dictated by the ratio of the dissociation constants K_{d1} and K_{d2} . This ratio should stay constant even if the enzyme to DNA ratio is increased above one. Fig. 5A shows that the amplitude of the slowest phase decreases with increasing enzyme to DNA ratios providing evidence against this model. We conclude that the presence of two different DNA binding sites does not account for the data.

The existence of two non-interconverting enzyme species is not sufficient to account for the observed DNA binding and dissociation kinetics.

We show in the Results and Discussion and elsewhere in the Supplementary Results that the DNA binding and dissociation kinetics in the presence of AMPPNP and Mg^{2+} is consistent with a model that postulates the existence of two enzyme species (E_1 and E_2 ; Scheme S5A) and inconsistent with models with only one form of the enzyme. The two enzyme species are allowed to interconvert in this model. Here we test if a model in which the two species are not allowed to interconvert can also account for the data. Distinguishing between those models is important because the two enzyme species could differ covalently or conformationally. If the two species are covalently different they would not be expected to interconvert on the time scales of the DNA binding and dissociation experiments. Thus, ruling this model out would provide strong evidence against covalent heterogeneity of the enzyme as the source of the complex DNA binding and release kinetics.

We consider the mechanism with two enzyme species E_1 and E_2 that cannot interconvert (Scheme S5B) and test its consistency with the data. If one of the two species bound and released DNA faster than the other species, multiphasic DNA binding and release time traces could be observed. This model predicts that both the fast and the slow DNA binding phase are second order reactions -i.e., that their observed rate constants increase if the enzyme and DNA concentrations are increased. Contrary to the prediction, the rate constants for the slowest association phase did not change when the enzyme and DNA concentrations were both increased from 50 to 120 nM (0.04 s^{-1} and 0.05 s^{-1} ; Fig. 5A, S3A and analysis not shown), providing strong evidence against this model. Moreover, according to the model, two enzyme-DNA complexes would build up -one with the rate constant of the fast and one with that of the slow association phase ($k_3 = 0.04 - 0.13\text{ s}^{-1}$ for the slow phase; Fig. 5A). However, the fast and the slowly dissociating enzyme species are populated significantly faster than 0.13 s^{-1} : after 65 ms, the fast and 50% of the slowly dissociating enzyme-DNA species have already built up (Fig. 6A). The corresponding rate constant ($\ln(2) / 65\text{ ms}$

= 11 s⁻¹) is significantly faster than 0.13 s⁻¹, inconsistent with the model of two non-interconverting enzyme species.

The slow kinetic phase in DNA dissociation traces in Ca²⁺ corresponds to DNA religation

As described in the Results and Discussion, the DNA dissociation kinetics in Ca²⁺ (Fig. 3B) is biphasic with the rate constant of the slow phase matching the rate constant for religation of the breaks in the DNA. This similarity prompted us to assign the slow phase in the dissociation kinetics to religation of DNA strand breaks. In the simplest case, the amplitude of the slow dissociation kinetic phase would also match the fraction of covalent complexes. However, the amplitude of this phase ($A_1 = 70\%$) moderately exceeds the estimated fraction of covalent complexes under these conditions (~55% total, with 45% of the enzyme-DNA complexes expected to have a double strand break and 10% a single strand break; Figs. S1B & 4D).

This discrepancy could have its origin in a number of non-mutually exclusive effects. First, the low anisotropy signal may not allow accurate distinction between the phases. Second, not all enzyme-DNA complexes may have the same fluorescence anisotropies; indeed, evidence for such a difference is presented in the Results and Discussion. Finally, an additional phase could be present in the dissociation kinetics that is either not resolvable by the data or is “hidden” as part by the religation kinetics. Indeed, an additional phase derived from the isomerization step K'_{iso} (Scheme 1) with a rate constant in between the k_1 and k_2 is likely present by analogy to data obtained in Mg²⁺ (Fig. 3A). In summary, noise in the data and small limitations of the model we applied to interpret the data are the likeliest cause of the discrepancy. While individual values for rate constants of K_{iso} and K'_{iso} in Table 1 may change in these cases, conclusions throughout are unaffected with regards to the exact origin of the discrepancy.

DNA cleavage time courses obtained with varying enzyme to DNA ratios suggest the existence of two interconverting enzyme species

As discussed in the Results and Discussion, the decreasing observed rate constant for DNA cleavage with increasing DNA to enzyme ratios with AMPPNP present (Fig. S1) provides strong evidence for the existence of two enzyme species. In a model in which the two species can interconvert, cleavage could be slower for one enzyme species (E', Scheme 1) than for the other (E) due to slower DNA binding or an isomerization step before DNA binding (K'_d or K_{iso} , in Scheme 1). Regardless from which species the cleavage reaction is initiated, both species have to go through the same cleavage step in this model. Conversely, if the two species do not interconvert, they would have to go through distinct DNA cleavage steps that could have different rate and equilibrium constants. Here we test if the enzyme species have distinct or identical cleavage steps. To this end we isolate and compare the cleavage equilibrium and the religation kinetics of the fast and the slowly cleaving enzyme population.

If the cleavage steps are identical for both species, two predictions have to be met. First, the fast cleaving enzyme population should reach the same maximal extent of cleavage as the slowly cleaving enzyme but much faster. Second, the observed DNA religation rate constant should be independent of which species was being isolated during the forward (cleavage) reaction.

We noted in the Results and Discussion that cleavage by the fast binding enzyme can be isolated when enzyme concentrations in large excess of the DNA concentrations are used. Conversely, cleavage by the slowly binding fraction can be probed using stoichiometric concentrations of enzyme and DNA. The maximal extent of cleavage remained constant when the enzyme exceeded or was stoichiometric to the DNA concentration (Fig. S1B). Moreover, the cleavage equilibrium was reached faster (after ca. 10 s) with enzyme in large excess of the DNA than with stoichiometric enzyme and DNA (ca. 100 s; Fig. S1A and data not shown), fulfilling the first prediction of the model.

The second prediction of the model was tested by measuring the observed DNA religation rate constants in pulse chase reactions. The religation kinetics of the two species was isolated by kinetically populating DNA strand breaks selectively by the fast or by the slowly cleaving enzyme before the chase was applied. Identical religation kinetics was observed for both species (Fig. S4), fulfilling the second prediction of the model.

In conclusion, the slowly and the fast cleaving enzyme species go through cleavage steps that have identical properties. The two species can presumably interconvert and this interconversion step is included in the overall model presented in the main text.

The rate limiting step of the DNA cleavage reaction

The data presented in the Results and Discussion allow us to infer which step is rate limiting. The rate limiting step for cleavage of the first or second DNA strand can be placed after DNA binding because the DNA dissociation rate constant ($k_{off} = 120 \text{ s}^{-1}$; Table 1) is significantly faster than the observed rate constant for cleavage of the first strand ($k_{obs} = 0.3 \text{ s}^{-1}$; Fig. S8B). Moreover, the rate limiting step for cleavage of the second DNA strand has to have occurred prior to the actual second chemical step as follows. If the second chemical step were rate limiting, the single cut intermediate would initially build up and then be depleted over time, but such a buildup is not observed. Lastly, the isomerization step before cleavage of the first strand cannot be rate limiting for the two cleavage events; in this model, single and double cut cleavage products would form with the same observed rate constant. Together, the data require that the rate limiting step for cleavage for both strands be concomitant to cleavage of the first strand. The global analysis of the data confirms the location of the rate limiting step (see the free energy profile in Fig. 8).

The kinetic lag for formation of single strand breaks in the presence of AMPPNP indicates the presence of a conformational step subsequent to association between enzyme and DNA

As explained in the Results and Discussion, there is a lag in the formation of single strand breaks in the presence of AMPPNP (Fig. 7, right panel). The lag could have its origin in a step that precedes DNA binding (k_{iso} in Scheme 1, model 1), in a partially rate limiting binding step (k_{on} , model 2), or in a step between DNA binding and cleavage of the first strand (k'_{iso} , model 3). We show in the Results and Discussion that simple models that do not include any of these steps cannot account for the presence of the lag whereas model 3 can. Here we evaluate and rule out models 1 and 2.

Model 1 postulates that a fraction of the enzyme must undergo a conformational change before it can bind DNA. It predicts that the kinetic lag disappears with increasing enzyme to DNA ratios. However, the lag was unaffected when the enzyme to DNA ratio was increased from 300:1 to 900:1 (Fig. 7, right panel).

Model 2 postulates that DNA binding is partially rate limiting for cleavage. Increasing the enzyme concentration would then make the association step less rate limiting, and the size of the lag would decrease in this model. However, the lag remained constant when the enzyme concentration was varied, providing strong evidence against this model (Fig. 7). Moreover, theoretical consideration (see section above) and quantitative kinetic modeling ruled out that the binding step is part of the rate limiting step (Fig. 7, dotted line and analysis not shown; see also free energy profile in Fig. 8).

The DNA cleavage and the fluorescence anisotropy assay monitor different subsets of conformational changes: Evidence for a thermodynamically favorable and an unfavorable conformational change subsequent to DNA binding

The rate constants k'_{iso} and k'_{-iso} obtained from the DNA cleavage and from the fluorescence anisotropy data are not identical (Tables 1 & 2). Here we discuss the

origin of these differences. We suggest that the conformational change these rate constants describe (k'_{iso}) is likely made up of multiple substeps and that the differences in the values of the rate constants arise because the anisotropy assay is limited to the detection of only thermodynamically favorable conformational steps.

There are two differences between the two assays we employed to extract values for k'_{iso} and k'_{-iso} . First, the divalent metal ion used to determine the rate constants differed (Mg^{2+} vs. Ca^{2+}). Second, the anisotropy assay but not the DNA cleavage assay is limited in detecting only enzyme-DNA species that accumulate. Either (or both) difference(s) could cause the apparent discrepancy in the rate constants. The following paragraphs discuss these possibilities in detail, and we provide evidence against the former possibility.

To extract values for k'_{iso} and k'_{-iso} , Mg^{2+} had to be used in the fluorescence anisotropy assay (see Results and Discussion), whereas DNA cleavage could only be measured accurately in Ca^{2+} . The differences in the rate constants could therefore be explained by the difference in the divalent metal ion employed in the two assays. However, the values of the rate constants describing the isomerization in the absence of DNA (k_{iso} and k_{-iso}) are the same in Ca^{2+} and Mg^{2+} , within 50% (Fig. 5 & analysis not shown). The similarity of these constants suggests that the values for the isomerization rate constants in the presence of DNA (k'_{iso} and k'_{-iso}) in Mg^{2+} and Ca^{2+} are also similar, arguing against this model.

Alternatively, the difference between the rate constants obtained from the two assays could arise from an inherent limitation of the fluorescence anisotropy assay: this assay can only detect steps subsequent to DNA binding that are thermodynamically favorable as only favorable steps lead to accumulation of additional enzyme-DNA species. Indeed, the conformational step observed by the anisotropy data is thermodynamically favorable ($k'_{iso} > k'_{-iso}$, Table 1). The DNA cleavage assay on the other hand is not limited towards thermodynamically favorable steps. In fact, the DNA cleavage data herein and in a previous study predict an unfavorable isomerization step ($k'_{iso} < k'_{-iso}$; Table 2 and [1]). It is possible that this unfavorable step is made up of two substeps: one step that is favorable (the step

detected by the anisotropy data) and a subsequent thermodynamically unfavorable step. Thus, our working model is that both steps together make up the overall unfavorable isomerization step determined from the DNA cleavage data described in the main text and summarized in Scheme 2.

In the main text we predict that closure of the ATPase domains is one of the conformational changes that take place after binding and before cleavage of DNA. Given the physical separation between the ATP binding modules and the active site for DNA cleavage (Fig. 1), it may not be surprising if the information about closure of the ATPase gate is relayed to the cleavage domains by a number of smaller conformational changes, accounting for the presence of substeps suggested above.

Determining the steps in the thermodynamic and kinetic framework for DNA cleavage that mediate the observed DNA strand cleavage cooperativity.

As explained in the Results and Discussion, cleavage of the two strands of the DNA exhibits positive cooperativity: the intermediate that bears only one strand break resolves most of the time to either an uncut or a double cut intermediate (positive thermodynamic cooperativity) and cleavage of the second strand is fast after the first cut has been introduced (positive kinetic cooperativity). We suggest in the Results and Discussion that non-chemical steps in the framework are responsible for the cooperativity effects. If non-chemical steps fully mediate the cooperativity, the (microscopic) rate and equilibrium constants of the two chemical steps would be the same. In principle, three locations for steps mediating the cooperativity are possible: after DNA binding and before cleavage of the first strand (Model 1), after cleavage of the first strand and before cleavage of the second (Model 2) and after cleavage of the second strand (Model 3). In this section, we consider the possible contributions of steps at these locations towards the observed DNA strand cleavage cooperativity. The analysis demonstrates that a step after DNA binding and before cleavage of the first strand is necessary and sufficient to explain the observed kinetic and thermodynamic strand cleavage cooperativity, providing evidence for Model 1 and against the other models.

Model 1: It is possible that a comparatively slow and thermodynamically unfavorable step that occurs prior to cleavage of the first strand (K'_{iso}) could be the reason why the observed formation of the first cut is apparently slower and less thermodynamically favorable than formation of the second cut. Indeed such a model results in a good fit of the DNA cleavage data (lines in Figs. 4D and 7) demonstrating that K'_{iso} can be the sole source for the observed strand cleavage cooperativity.

Model 2: A step that is located after cleavage of the first but before cleavage of the second strand can only lower the observed thermodynamic cooperativity as shown mathematically below. For a derivation we consider a simplified mechanism of the DNA cleavage reaction (Scheme S7) in which a conformational change K_{conf} occurs between the two strand cleavage steps (K_{clvg}). If K_{conf} were the sole source of the observed thermodynamic cooperativity, the equilibria of the two cleavage steps (K_{clvg}) share the same values. The DNA binding step can be neglected thermodynamically when conditions are used under which all DNA is bound by the enzyme. The association step is therefore omitted in Scheme S7. Below we derive an equation for the observed thermodynamic cooperativity in dependence of K_{conf} . We show with this equation that K_{conf} in Scheme S7 cannot account for the observed thermodynamic cooperativity.

The *observed* equilibrium for formation of the first cut ($K_{obs, single cut}$) is the sum of the concentrations of all single cut intermediates over the concentration of the enzyme-DNA encounter complex (Eq. 5).

$$K_{obs, single cut} = ([E_{SP}] + [E'_{SP}]) / [E_{SS}] \quad (5)$$

Similarly, the *observed* equilibrium for formation of the second cut ($K_{obs, double cut}$) is the concentration of the double cut intermediate over the sum of the concentrations of all single cut intermediates (Eq.6).

$$K_{obs, double cut} = [E'_{PP}] / ([E_{SP}] + [E'_{SP}]) \quad (6)$$

The observed thermodynamic cooperativity (*ThermCoop*) is defined as the ratio of the observed equilibria for formation of the first and the second cuts (Eq. 7).

$$ThermCoop = K_{obs, double\ cut} / K_{obs, single\ cut} \quad (7)$$

With $K_{conf} = [E'_{SP}] / [E_{SP}]$ and $K_{clvg} = [E_{SP}] / [E_{SS}] = [E'_{PP}] / [E'_{SP}]$ we can now write

$$ThermCoop = K_{conf} / (1 + K_{conf})^2 \quad (8)$$

Inspection of Eq. 8 shows that *ThermCoop* assumes values that are always below one. In other words, positive thermodynamic cooperativity (*ThermCoop* > 1) cannot be achieved with the mechanism shown in Scheme S7. A step after cleavage of the first and before cleavage of the second strand can therefore be ruled out as the source of the observed positive thermodynamic cooperativity.

Moreover, the mechanism shown in Scheme S7 cannot explain why strand cleavage after the first cut has been introduced is much faster than the observed formation of the first strand break. Thus, this mechanism also cannot account for the positive kinetic cooperativity of strand cleavage.

Model 3: A step subsequent to cleavage of the second strand could cause the observed positive thermodynamic cooperativity (Scheme S8). If this step is thermodynamically favorable, more DNA-enzyme complexes are pulled towards a state in which both DNA strands are cleaved thereby producing a greater observed equilibrium for cleavage of the second relative to the first strand. However, this mechanism cannot explain the observation that cleavage of the second strand is fast once the first strand is cleaved (positive kinetic cooperativity), because a step subsequent to the chemical step cannot accelerate the chemical step.

In summary, the analysis in this section demonstrates that a step after DNA binding and before cleavage of the first strand is implicated in mediating all or part of the observed kinetic and thermodynamic strand cleavage cooperativity. In addition, a

step after cleavage of the second strand could contribute to the observed thermodynamic but not kinetic cooperativity. Because the data do not require a step subsequent to cleavage of the second strand we do not include it in the simple, unifying model presented in the Results and Discussion, and we attribute the observed kinetic and thermodynamic cooperativity exclusively to the step K'_{iso} in Scheme 2A.

What are the conformational changes that take place during the isomerization steps?

The kinetic and thermodynamic data presented in the main text strongly suggest the existence of a conformational rearrangement of the enzyme prior to DNA binding and of the enzyme-DNA complex following DNA binding (K_{iso} and K'_{iso} , Scheme 1). Because the conformational steps are sensitive to the presence of AMPPNP, conformational changes known to be induced by AMPPNP binding are strong candidates for the isomerization steps. In this section we present an overview of previously identified structural rearrangements that take place upon nucleotide binding and discuss the possible roles of these rearrangements in transmitting information about the nucleotide state to the DNA cleavage reaction.

X-ray crystallography resolved two conformational changes induced by nucleotide binding at atomic resolution. They are depicted schematically in Scheme S4. The ATPase domains are composed of two modules: the ATP binding domains, also known as the GHKL domains, and the transducer domains that separate the GHKL modules from the DNA cleavage domains [2-5]. With nucleotides present the two GHKL domains can associate or “dimerize” (K_{Dimer} and K'_{Dimer} ; Scheme S4) [3,5-7]. Nucleotide binding also affects the relative orientation of the transducer to the GHKL domains. In the AMPPNP bound state the transducer docks against the GHKL domains, and a lysine residue of the transducer inserts itself into the ATP binding pocket where it contacts the γ -phosphoryl group (K_{Dock} and K'_{Dock}) [3,5-8]. Conversely, the transducer is undocked from the GHKL domains in the absence of nucleotides and in certain other nucleotide states [6-9]. The lysine residue is retracted and the

transducer domains are rotated away from the GHKL domains in this conformation. Docking resembles a rigid body motion of the two domains against each other [5-7,9].

Either docking of the transducer against the GHKL module (model 1), dimerization of the ATPase domains (model 2), docking and dimerization (model 3), or completely unrelated conformational changes (model 4) can in principle correspond to the isomerization steps that have been exposed by our kinetic dissection of the DNA cleavage reaction (K_{iso} and K'_{iso} , Scheme 1).

In model 1, docking alone, irrespective of the dimerization state, signals the nucleotide state to the DNA cleavage domains. The transducer domains can transmit the information about the nucleotide state to the DNA cleavage domains in two ways. Either the structure of the transducer domains or the relative orientation of the transducer to the DNA cleavage domains changes upon nucleotide binding. Crystallographic studies suggest that docking of the GHKL module against the transducer domain resembles a rigid body motion [6,8], providing no indication of a structural change of the transducer domain upon docking and arguing against the former possibility. Because the GHKL domains are thought not to directly contact the DNA cleavage domains [2,10,11], docking of the GHKL and transducer domains is not expected to affect the relative orientation of the transducer and DNA cleavage domains, arguing against the latter possibility.

The second and third models postulate that dimerization or dimerization in conjunction with docking mediates the crosstalk between the ATPase and DNA cleavage domains. Because access to the G-DNA binding site is provided by the ATPase domains, ATPase domain dimerization could be responsible for the hindered DNA binding and release in the enzyme conformation that predominates in the presence of AMPPNP (E'; Scheme 1). Thus, dimerization alone or dimerization in conjunction with docking are strong candidates for the isomerization steps we discovered in the DNA cleavage framework.

In summary, current structural data point to the dimerization of the ATPase domains as the simplest and most likely candidate for the isomerization steps that take place during the cleavage reaction. Nevertheless, conformational changes that have yet

to be discovered and are unrelated to dimerization and docking could couple nucleotide binding to DNA cleavage (model 4).

SUPPLEMENTARY REFERENCES

1. Mueller-Planitz F, Herschlag D (2007) DNA topoisomerase II selects DNA cleavage sites based on reactivity rather than binding affinity. *Nucleic Acids Res* 35: 3764-3773.
2. Corbett KD, Benedetti P, Berger JM (2007) Holoenzyme assembly and ATP-mediated conformational dynamics of topoisomerase VI. *Nat Struct Mol Biol* 14: 611-619.
3. Wigley DB, Davies GJ, Dodson EJ, Maxwell A, Dodson G (1991) Crystal structure of an N-terminal fragment of the DNA gyrase B protein. *Nature* 351: 624-629.
4. Ali JA, Jackson AP, Howells AJ, Maxwell A (1993) The 43-kilodalton N-terminal fragment of the DNA gyrase B protein hydrolyzes ATP and binds coumarin drugs. *Biochemistry* 32: 2717-2724.
5. Classen S, Olland S, Berger JM (2003) Structure of the topoisomerase II ATPase region and its mechanism of inhibition by the chemotherapeutic agent ICRF-187. *Proc Natl Acad Sci U S A* 100: 10629-10634.
6. Wei H, Ruthenburg AJ, Bechis SK, Verdine GL (2005) Nucleotide-dependent domain movement in the ATPase domain of a human type IIA DNA topoisomerase. *J Biol Chem* 280: 37041-37047.
7. Corbett KD, Berger JM (2003) Structure of the topoisomerase VI-B subunit: implications for type II topoisomerase mechanism and evolution. *Embo J* 22: 151-163.
8. Corbett KD, Berger JM (2005) Structural dissection of ATP turnover in the prototypical GHL ATPase TopoVI. *Structure* 13: 873-882.
9. Lamour V, Hoermann L, Jeltsch JM, Oudet P, Moras D (2002) An open conformation of the *Thermus thermophilus* gyrase B ATP-binding domain. *J Biol Chem* 277: 18947-18953.
10. Benedetti P, Silvestri A, Fiorani P, Wang JC (1997) Study of yeast DNA topoisomerase II and its truncation derivatives by transmission electron microscopy. *J Biol Chem* 272: 12132-12137.
11. Schultz P, Olland S, Oudet P, Hancock R (1996) Structure and conformational changes of DNA topoisomerase II visualized by electron microscopy. *Proc Natl Acad Sci U S A* 93: 5936-5940.
12. Mueller-Planitz F, Herschlag D (2006) Interdomain communication in DNA topoisomerase II: DNA binding and enzyme activation. *J Biol Chem* 281: 23395-23404.

Table S1 **Oligodeoxyribonucleotides used to assemble DNA duplexes**

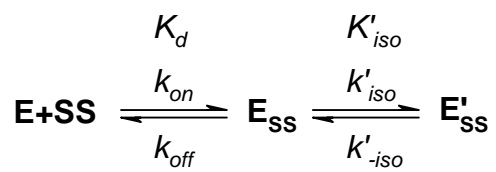
Name	Sequence (5' – 3')
Oligo ₄₀ top	TGAAATCTAACAATGCGCTCATCGTCATCCTCGGCACCGT
Oligo ₄₀ bottom	ACGGTGCCGAGGATGACGATGAGCGCATTGTTAGATTTCA
Oligo ₄₀ top-ROX ^a	ROX - TGAAATCTAACAATGCGCTCATCGTCATCCTCGGCACCGT
Oligo ₃₄ ^b	CCGAGGATGACGATGAGCTCATCGTCATCCTCGG
Oligo ₃₄ -dumbbell ^c	CTCATCGTCATCCTCGG - Sp9 - CCGAGGATGACGATGAGCTCATCGTCATCCTCGG - Sp9 - CCGAGGATGACGATGAG

^a ROX: 6-Carboxy-X-rhodamine.

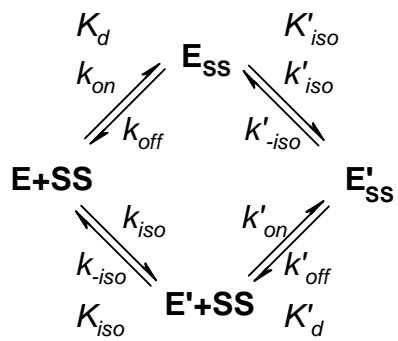
^b Oligo₃₄ is self-complementary, so top and bottom strands are identical.

^c Sp9: triethylene glycol spacer; the oligodeoxyribonucleotide is self-complementary.

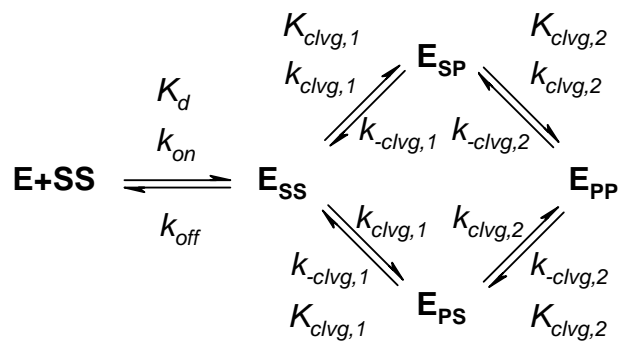
Scheme S1



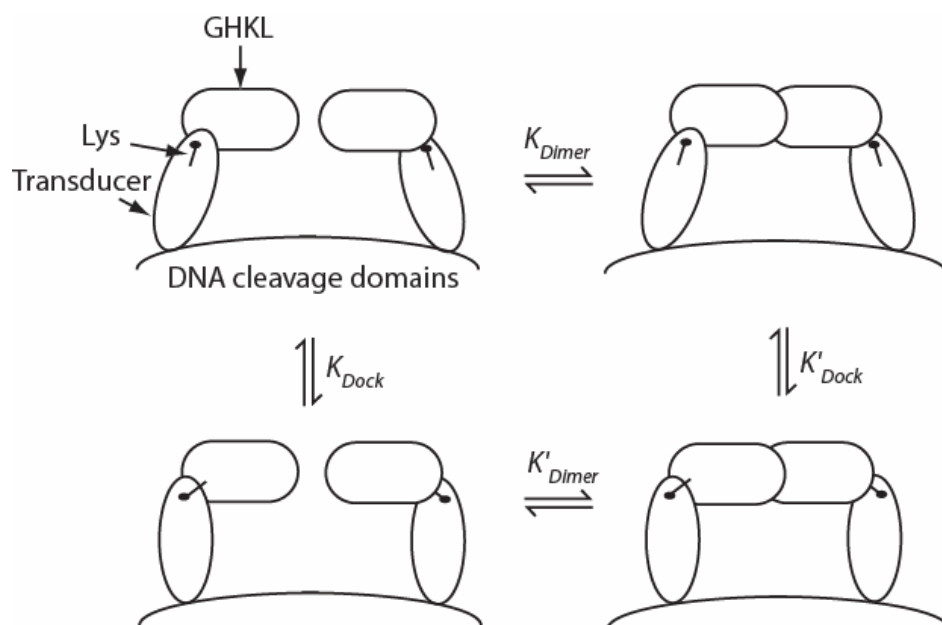
Scheme S2



Scheme S3

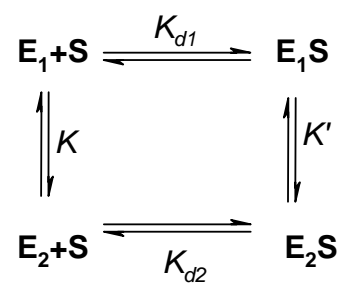


Scheme S4

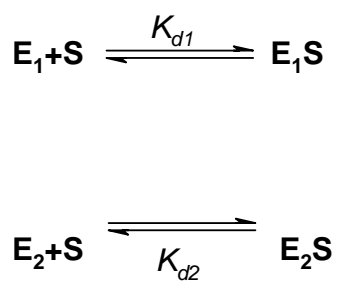


Scheme S5

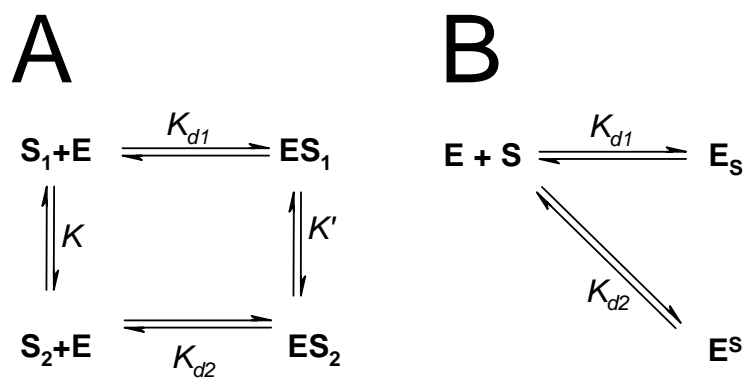
A



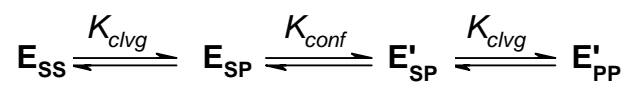
B



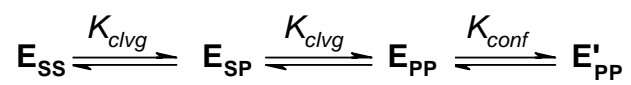
Scheme S6



Scheme S7



Scheme S8



Supplementary Figure Legends

Fig. S1: Two enzyme species that cleave DNA with different observed rate constants can be detected in the presence of AMPPNP (closed symbols) but not in its absence (open symbols). Saturating concentrations of enzyme (240 nM) were rapidly mixed with varying concentrations of the 40 bp DNA duplex (Table S1) in 10 mM Ca^{2+} and DNA cleavage was followed over time. The time courses were fit to a single exponential expression. The observed rate constant (A) and the extent of cleavage at equilibrium (B) were plotted over the ratio of enzyme to DNA. In the absence of nucleotides, the observed rate constant did not vary over the entire range of DNA to enzyme ratios tested, averaging at 0.08 s^{-1} . Similarly, the fraction of cleavage was constant with enzyme in excess of DNA. As expected and previously observed [12], less cleavage was detected when the DNA concentration exceeded the enzyme concentration because the available G-DNA binding sites have been titrated by DNA, and additional DNA cannot be cleaved by the enzyme. In the presence of saturating concentrations of AMPPNP (0.5 mM), DNA is cleaved with observed rate constants of $0.23 - 0.25 \text{ s}^{-1}$ with enzyme in large excess of DNA. The observed rate constant decreased to 0.035 s^{-1} when approximately stoichiometric concentrations of enzyme and DNA were used. The same rate constant (0.035 s^{-1}) was obtained when stoichiometric, but five-fold lower DNA and enzyme concentrations were used (data not shown). Midpoint of the curve: $[\text{DNA}:\text{E}]_{1/2} = 0.15$.

Fig. S2: Global fit of DNA binding (left panel) and dissociation kinetic traces (right panel) obtained in Mg^{2+} to Scheme S1. The kinetic traces used for the fit were taken from Figs. 2A & 3A (see figure legend for experimental conditions). In addition, a DNA binding kinetic trace obtained at 120 nM enzyme and 120 nM DNA (cyan) was included in the fit. The individual kinetic traces are offset from one another for presentation purposes. Black lines: global fit. Global fit parameters are summarized in Table 1.

Fig. S3: Global fit of DNA binding (left panel) and dissociation kinetic traces (right panel) obtained in the presence of 10 mM Mg^{2+} and 0.5 mM AMPPNP to Scheme S2. The kinetic traces used for the fit were taken from Figs. 5A & 6A (see figure legends for experimental conditions). In addition, a DNA binding kinetic trace obtained at 120 nM enzyme and 120 nM DNA (cyan) was included in the fit. All DNA binding kinetic traces were corrected for the downward kinetic phase detected at an enzyme to DNA ratio of 9:1 (blue trace in Fig. 5A) by adding a single exponential with the amplitude and observed rate constant of this downward phase to the data. The individual kinetic traces in the left panel are offset from one another for presentation purposes. Black lines: global fit. Global fit parameters are summarized in Table 1.

Fig. S4: The two enzyme populations that were detected in Fig. S1 in the presence of AMPPNP religate DNA with the same observed rate constants. DNA religation was measured in pulse chase experiments. The enzyme (240 nM), preincubated with 10 mM Ca^{2+} and 0.5 mM AMPPNP, was allowed to cleave ^{32}P -labeled 40 bp DNA duplex (3 nM, except *black diamonds*: 300 nM; see Table S1 for the DNA sequence) for a variable amount of time (*green triangles*: 2 s; *blue circles*: 5 s; *red squares*: >6 min; *black diamonds*: >6 min) before the reaction was “chased” with excess unlabeled DNA at time zero. Varying the time the enzyme is allowed to cleave DNA before the chase serves to isolate the religation kinetics of the fast or the slowly cleaving enzyme (E and E', respectively; Scheme 1; Fig. S1). The religation time courses are indistinguishable from one another with an observed rate religation rate constant of $0.018 \pm 0.02 \text{ s}^{-1}$ (single exponential fit; average and standard deviation of the four time courses), indicating that the two enzyme populations detected in Fig. S1 religate DNA with the same observed rate constant.

Fig. S5: The unifying model predicts religation rate constants within an accuracy of 50%. Religation time courses for DNA dumbbells were obtained as described in Figs. 4 & S4. *Red circles*: single strand breaks; *blue squares*: double strand breaks. Each time course is fit to an unconstrained single exponential expressions (k_{obs} ; solid lines)

and a single exponential with a rate constant set to a value predicted by the global analysis of the DNA cleavage time courses (k_{pred} ; dashed lines). A) DNA religation in the absence of nucleotides. Best-fit values: $k_{obs, single\ cut} = 0.056\ s^{-1}$, $k_{obs, double\ cut} = 0.048\ s^{-1}$. Rate constant predicted by the global analysis: $k_{pred, single\ cut} = k_{pred, double\ cut} = 0.07\ s^{-1}$ (Fig. 4D and analysis not shown). B) DNA religation in the presence of 0.5 mM AMPPNP. Best-fit values: $k_{obs, single\ cut} = 0.028\ s^{-1}$, $k_{obs, double\ cut} = 0.024\ s^{-1}$. Rate constant predicted by the global analysis: $k_{pred, single\ cut} = k_{pred, double\ cut} = 0.02\ s^{-1}$ (Fig. 7 and analysis not shown).

Fig. S6: Global fit of DNA cleavage time courses in the absence (open symbols, broken lines) and presence of AMPPNP (closed symbols, solid lines) to Scheme 2A. The data were taken from Figs. 4 & 7. Right panel: magnification of the pre-steady state phase of the time courses. Values of k_{on} and k_{off} were set to those determined by stopped flow fluorescence anisotropy (Table 1). The chemical steps were enforced to have the same rate constants ($k_{clvg,1} = k_{clvg,2}$ and $k_{-clvg,1} = k_{-clvg,2}$) and AMPPNP was allowed to affect only one rate constant (k'_{-iso}) in the fit. Best fit parameters: $k'_{iso} = 1.2\ s^{-1}$, $k'_{-iso, no\ nucleotide} = 87\ s^{-1}$, $k'_{-iso, AMPPNP} = 12\ s^{-1}$, $k_{clvg,1} = k_{clvg,2} = 5.9\ s^{-1}$, $k_{-clvg,1} = k_{-clvg,2} = 0.60\ s^{-1}$.

Fig. S7: Cleavage specificity of the blunt-end 34 bp duplex (Table S1). Trace amounts of radio-labeled 34 bp duplex were mixed with reaction buffer or enzyme and the extent of cleavage analyzed as described in the Experimental Procedures. Under conditions that allow for single nucleotide resolution (data not shown), a single cleavage product is observed (specificity >95%). Smearing of the band belonging to the uncleaved DNA oligonucleotide is due to residual secondary structure, a result of the self-complementarity of the oligodeoxynucleotide. This residual structure can be disrupted using strongly denaturing conditions (40% formamide, 7 M urea; data not shown).

Fig. S8: Enzyme concentrations above 300 nM are saturating with respect to the DNA cleavage kinetics of nucleotide-free enzyme. A) DNA cleavage time courses with trace amounts of dumbbell duplex DNA and 300 nM (*red*) and 900 nM enzyme (*blue*) were obtained as in Fig. 4. The progress curves for the formation of the single strand break (*circles*) and the double strand break (*squares*) were fit to a single exponential expression (*lines*). B) The observed rate constant (k_{obs}) from the fits in A) plotted versus enzyme concentration. Increasing the enzyme concentration three-fold, from 300 to 900 nM, had only a modest (10%) effect on the observed rate constants, indicating saturation of enzyme.

Figure S1

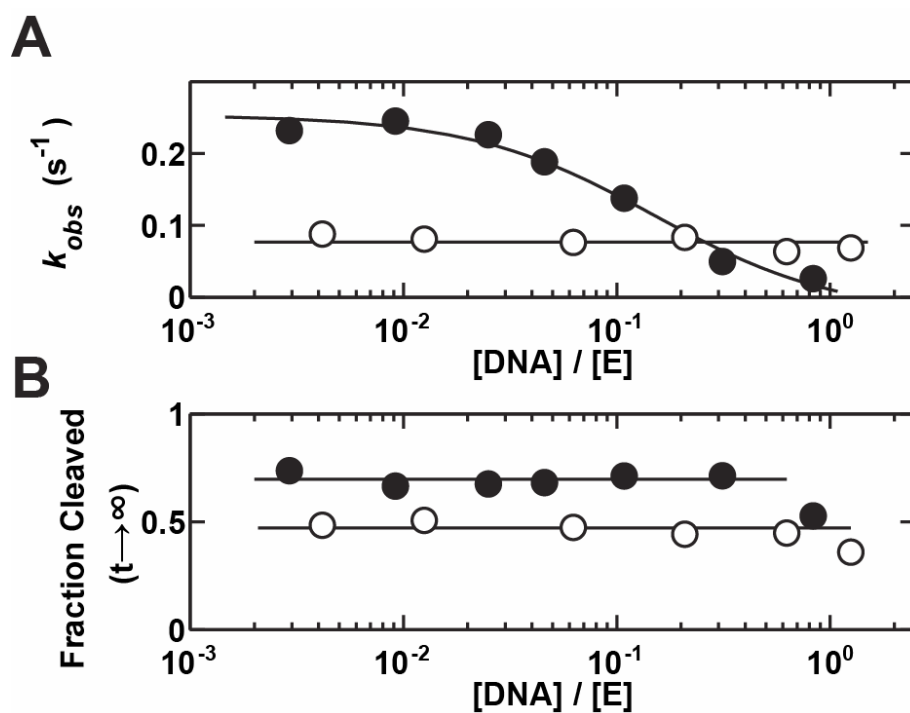


Figure S2

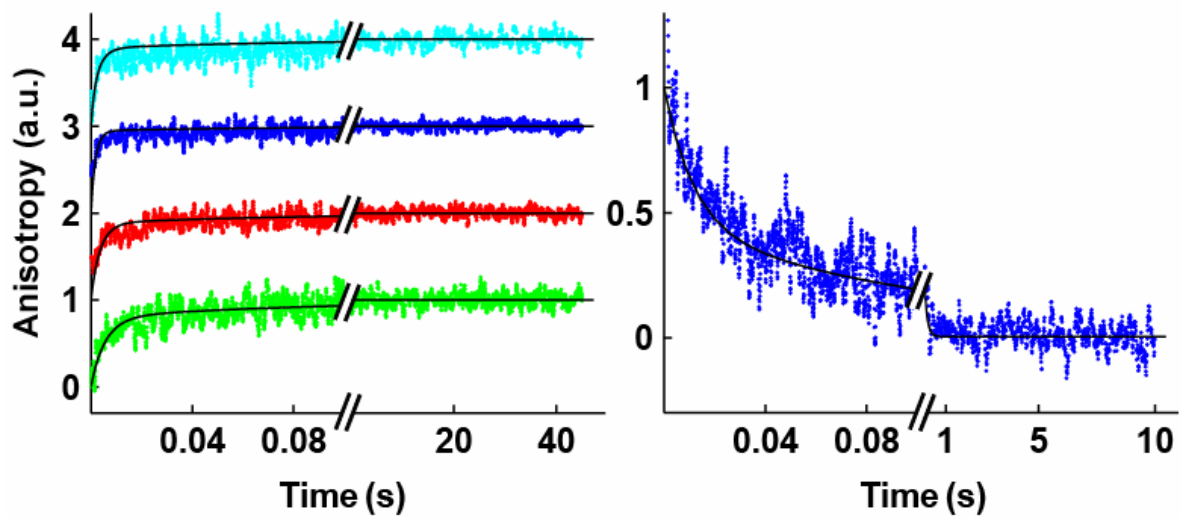


Figure S3

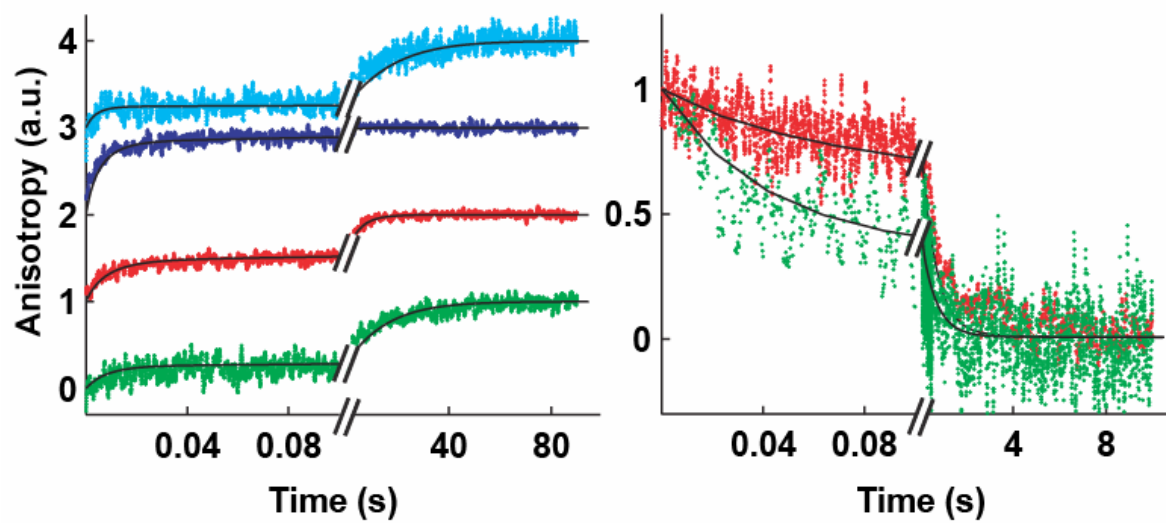


Figure S4

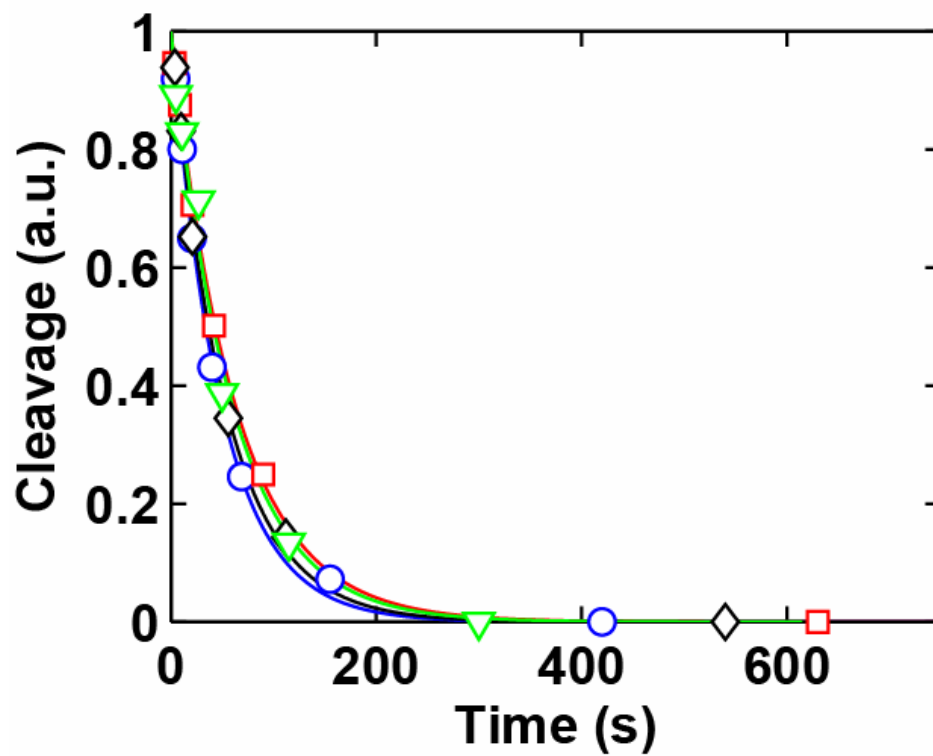


Figure S5

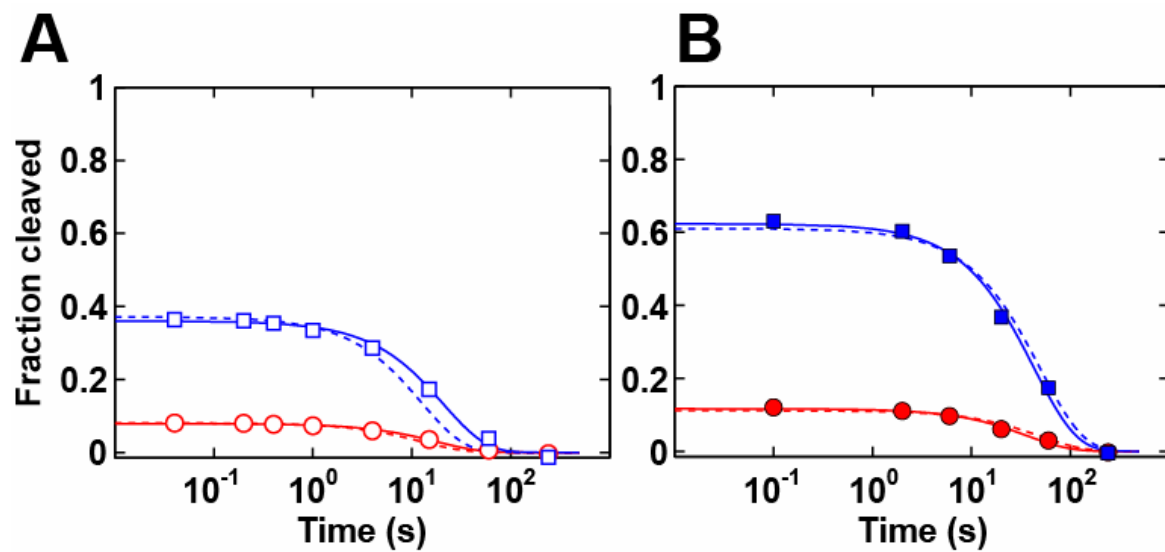


Figure S6

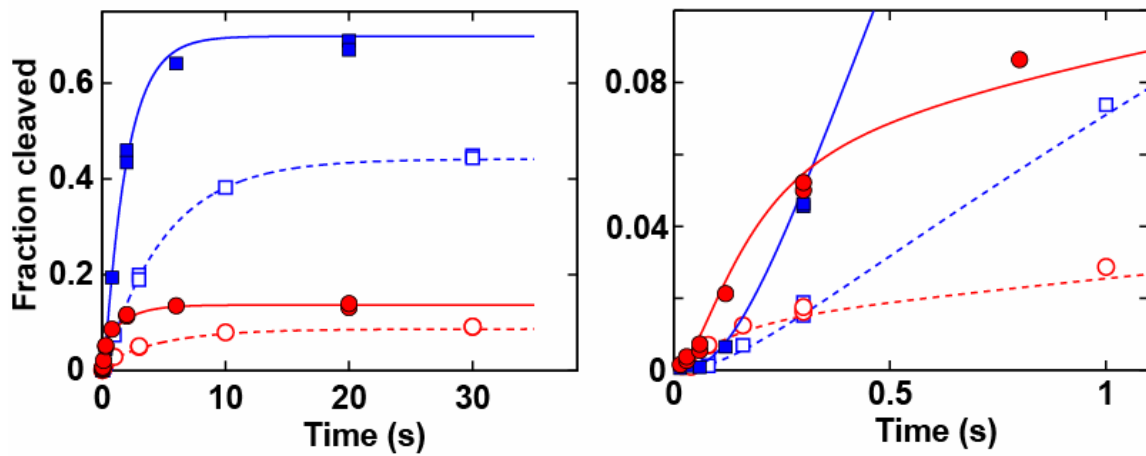


Figure S7

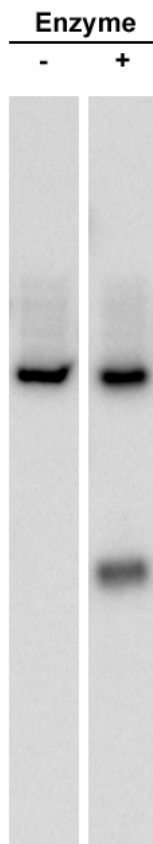


Figure S8

